frontiers in Earth Science

ORIGINAL RESEARCH
published: 06 December 2021
doi: 10.3389/feart.2021.784812

Northward Growth of the West Kunlun Mountains: Insight From the Age–Elevation Relationship of New Apatite Fission Track Data

Dongliang Liu[1,2]*, Haibing Li[1,2], Chenglong Ge[2], Mingkun Bai[2], Yadong Wang[3], Jiawei Pan[1,2], Yong Zheng[1,2], Ping Wang[2,4], Fucai Liu[2] and Shiguang Wang[5]

[1]Southern Marine Science and Engineering Guangdong Laboratory (Guangzhou), Guangzhou, China, [2]Key Laboratory of Deep-Earth Dynamics of Ministry of Natural Resources, Institute of Geology, Chinese Academy of Geological Sciences, Beijing, China, [3]Northwest Institute of Eco-Environment and Resources, China Academy of Sciences, Lanzhou, China, [4]Geophysical Exploration Center, China Earthquake Administration, Zhengzhou, China, [5]National Institute of Natural Hazards, MEMC, Beijing, China

OPEN ACCESS

Edited by:
Yibo Yang, Institute of Tibetan Plateau Research (CAS), China

Reviewed by:
Tianyi Shen, China University of Geosciences Wuhan, China
Jingen Dai, China University of Geosciences, China

***Correspondence:**
Dongliang Liu
liudl2010@yahoo.com

Specialty section:
This article was submitted to Structural Geology and Tectonics, a section of the journal Frontiers in Earth Science

Received: 28 September 2021
Accepted: 22 November 2021
Published: 06 December 2021

Citation:
Liu D, Li H, Ge C, Bai M, Wang Y, Pan J, Zheng Y, Wang P, Liu F and Wang S (2021) Northward Growth of the West Kunlun Mountains: Insight From the Age–Elevation Relationship of New Apatite Fission Track Data. Front. Earth Sci. 9:784812. doi: 10.3389/feart.2021.784812

The Cenozoic collision between India and Asia promoted the widespread uplift of the Tibetan Plateau, with significant deformation documented in the Pamir Plateau and West Kunlun Mountains. Low-temperature thermochronology and basin provenance analysis have revealed three episodes of rapid deformation and uplift in the Pamir–West Kunlun Mountains during the Cenozoic. However, there is very little low-temperature thermochronology age–elevation relationship (AER) data on fast exhumation events in this area—especially in the West Kunlun Mountains— leading to uncertainty surrounding how these events propagated within and around the mountain range. In this study, we produced an elevation profile across granite located south of Kudi, Xijiang Province, China, to reveal its exhumation history. Apatite fission track AER data show that a rapid exhumation event occurred at ~26 Ma in the southern West Kunlun Mountains. When combined with published data, we interpret that the initial uplift events related to the India–Asia collision began in the central Pamir, southern West Kunlun, and northern West Kunlun regions during the Late Eocene, Oligocene, and Middle Miocene periods, respectively. Therefore, the Cenozoic northward growth process occurred from south to north around West Kunlun.

Keywords: apatite fission track, age-elevation relationship, West Kunlun Mountains, Tibetan Plateau, deformation, uplift

INTRODUCTION

The Cenozoic collision between India and Asia formed the Tibetan Plateau (TP, **Figure 1A**), a series of intracontinental orogenic belts (Tapponnier et al., 2001; Royden et al., 2008), and induced regional climatic change (Raymo and Ruddiman, 1992). The onset ages of the India–Asia collision in the western Himalaya syntaxis (WHS), central Tibet and eastern Himalayan syntaxis (EHS) remain debated (Leech et al., 2005; Hu et al., 2016). The WHS is dominated by the Pamir Plateau, which is comprised of the northern Pamir, central Pamir, and southern Pamir (**Figure 1B**) domains. The northern Pamir has Asian affinity, whereas the central and southern Pamir regions have Cimmerian Gondwanan affinity (Burtman and Molnar, 1993; Li et al., 2020). The West Kunlun Mountains (WK), situated in the southeastern Pamir, are divided into the southern West Kunlun (SWK) and

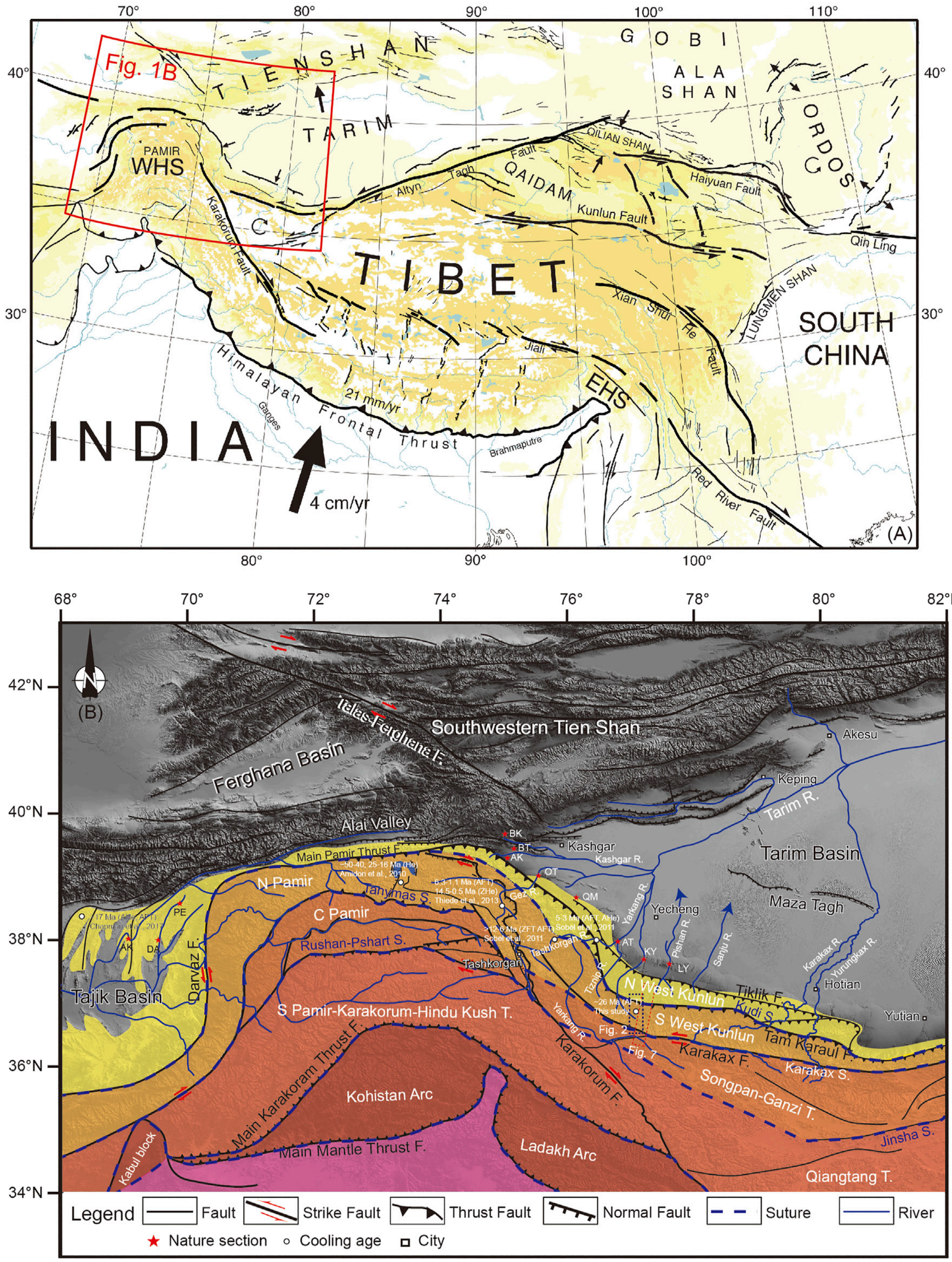

FIGURE 1 | (A) Location of the western Himalayan syntaxis (WHS) (modified from Tapponnier et al. (2001)). **(B)** Geomorphology and main faults in the Pamir–Southwestern Tien Shan. Red stars mark the main sites where magnetostratigraphy was performed in the southwestern Tarim and Tajik basins. Abbreviations are as follows: T, terranes; S., suture; F, fault; R, river; ZFT, zircon fission track age; ZHe, zircon (U–Th)/He age; AFT, apatite fission track age; AHe, apatite (U–Th)/He age; AK, Asku section; DA, Dashtijum section; PE, Peshtova section; BK, Baxbulak section; BT, Bora Tokay section; AK, Akqiy section; OT, Oytag section; QM, Qimugen section; AT, Aertashi section; KY, Kekeya section; and LY, Keliyang section).

northern West Kunlun (NWK) regions. These three parts of the Pamir extend to the southeast and correspond to the SWK, Songpan-Ganzi Terrane, and Qiangtang Terrane (**Figure 1B**; Robinson et al., 2004; Cowgill, 2010). Together, these domains are known as the Pamir–WK. The Cenozoic and pre-Cenozoic geological evolution of the Pamir–WK has been a topic of significant scientific focus over the past 20 years (Robinson et al., 2004; Cowgill, 2010; Li et al., 2020; Cai et al., 2021).

Low-temperature thermochronology is widely used to constrain the cooling histories of plateaus and mountain ranges (Reiners et al., 2005; Guenthner et al., 2013). Moreover, age–elevation relationship (AER) data are extremely valuable for defining the denudation and relief history in a locality, especially when an AER has a transform point (Braun, 2002; Valla et al., 2010). Previous low-temperature thermochronological studies in the study region have shown that the Pamir–WK experienced three rapid exhumation events during the Cenozoic at ~50–40, ~25–16, and between ~10 Ma and the present day (Robinson et al., 2004; Robinson et al., 2007; Amidon and Hynek, 2010; Sobel et al., 2011; Wang et al., 2011; Carrapa et al., 2014; Li et al., 2019). Other studies have shown that a provenance change or increase in sediment flux occurred at ~40–30, ~26, and ~15 Ma (Jiang and Li, 2014; Tang et al., 2015; Blayney et al., 2016; Sun et al., 2016; Wang et al., 2019; Zhang et al., 2019; Sun et al., 2020; Li et al., 2021; Sakuma et al., 2021; Wang et al., 2021). The Paleogene paleotopography in the WK may therefore represent an ancient land surface (Li et al., 2019). Despite this work, it is uncertain how these tectonic events propagated within and around the mountain range. This uncertainty is exacerbated by the paucity of low-temperature thermochronology AER data that constrain the uplift and exhumation rates in this area, especially in the WK. In this study, we collected samples of granite profiles situated south of Kudi, Xijiang Province, China, and used the AER of the apatite fission track (AFT) data to reveal the exhumation history of the SWK. These data record a transformation point within the AER, which means an abrupt tectonic transition in the SWK. We then integrate these results with those of previous studies to interpret the Cenozoic growth history of the WK.

GEOLOGICAL SETTING

The Pamir–WK is broadly salient and has been displaced northward over the Tarim–Tajik basins along the Main Pamir thrust system and Darvaz fault (**Figure 1B**). The Pamir–WK can be divided into four tectonic terranes: the NWK, the northern Pamir–SWK, the central Pamir–Songpan-Ganzi, and the Southern Pamir–Karakorum–Hidu Kush–Qiangtang, which are separated by the Kudi suture, Tanymas-Karakax suture, and Rushan-Pshart-Jinsha suture, respectively (**Figure 1B**). The former two terranes have affinity to Asia, whereas the latter two terranes previously split away from the Gondwanan (Burtman and Molnar, 1993; Li et al., 2020). The southwestern Tien Shan was situated north of the Pamir–WK prior to the shortening of strata during the Cenozoic, with estimates of shortening between both domains ranging between ~50 and 100 km (Chen et al., 2018; Li et al., 2020) and ~300 km (Burtman and Molnar, 1993).

The WK is bordered by the Tarim Basin to the north, the Pamir Plateau to the northwest, and the Songpan-Ganzi terrane to the south. It is a mountainous region ~700 km long, ~100–130 km wide, and contains peaks up to ~7,600 m high. The Tarim Basin has an elevation of <1,500 m, while the frontal orogenic fold belt between the Tarim Basin and the Tiklik fault has an elevation of 1,500–2,500 m. To the south of the Tiklik fault, the WK itself has an elevation of 3,000–6,000 m. The WK can be divided into the northern and southern parts by the Kudi suture (**Figure 1B**), which formed due to the closure of the Proto-Tethys Ocean (Matte et al., 1996). The WK initially formed during the Paleozoic-Mesozoic and experienced a complex strike-slip to compressive evolution (Yin and Harrison, 2000; Arnaud et al., 2003; Laborde et al., 2019). The WK reached its current elevation due to reactivation of pre-existing faults during the Cenozoic India–Asia collision (Matte et al., 1996; Yin and Harrison, 2000; Jiang et al., 2013; Laborde et al., 2019).

To the north of the WK, the Tarim Basin contains extensive Mesozoic-Cenozoic deposits and has an average thickness of ~1,200 m. Today, the Tarim Basin is an endorheic basin surrounded by mountain ranges: the Pamir–WK to the southwest, the Altyn Tagh Mountains to the southeast, and the Tien Shan to the north. These ranges previously provided abundant sediment that infilled the Tarim Basin, with the Pamir–WK having been the main sedimentary provenance for the SW Tarim Basin during the Mesozoic–Cenozoic, especially during the Cenozoic (Jiang and Li, 2014; Li et al., 2021). The Mesozoic strata in the SW Tarim Basin include Jurassic (Shalitashi, Kansu, Yangye and Kuzigongsu Formations) and Cretaceous (Kezilesu and Yengisar Groups) sediments (Sobel, 1999), and the Cenozoic strata include the Kashi Group (Aertashi, Qimugen, Kalatar, Ulagen and Bashibulake Formations), Wuqia Group (Keziluoyi, Anjuan and Pakabulake Formations), Artux Formation and Xiyu Formation (Jia et al., 2004; Liu et al., 2017a).

SAMPLING AND METHODS

Geological mapping and sampling were performed over several years in the WK in collaboration with the China Geological Survey. Survey routes were situated near the G219 highway, which runs from Xinjiang to Tibet, and granite samples were collected from southern Kudi. From north to south, this area consists of the NWK, SWK, and Songpan-Ganzi (**Figure 2**). The NWK includes Carboniferous and Mesoproterozoic rocks of the Changcheng System and Silurian and Ordovician granites. The SWK contains Mesoproterozoic rocks of the Changcheng System, alongside granite of various ages, and other deformed rocks. The Songpan-Ganzi terrane only shows exposed Silurian rocks. A topographic profile from the Songpan-Ganzi to the NWK shows that these three terranes attain maximum elevations exceeding 4,500, 3,000, and 2,700 m (**Figure 3**). The study regions contain several types of granite. Five samples (KDW52, KDW55, KDW60, KDW61, and KDW62) were collected from a

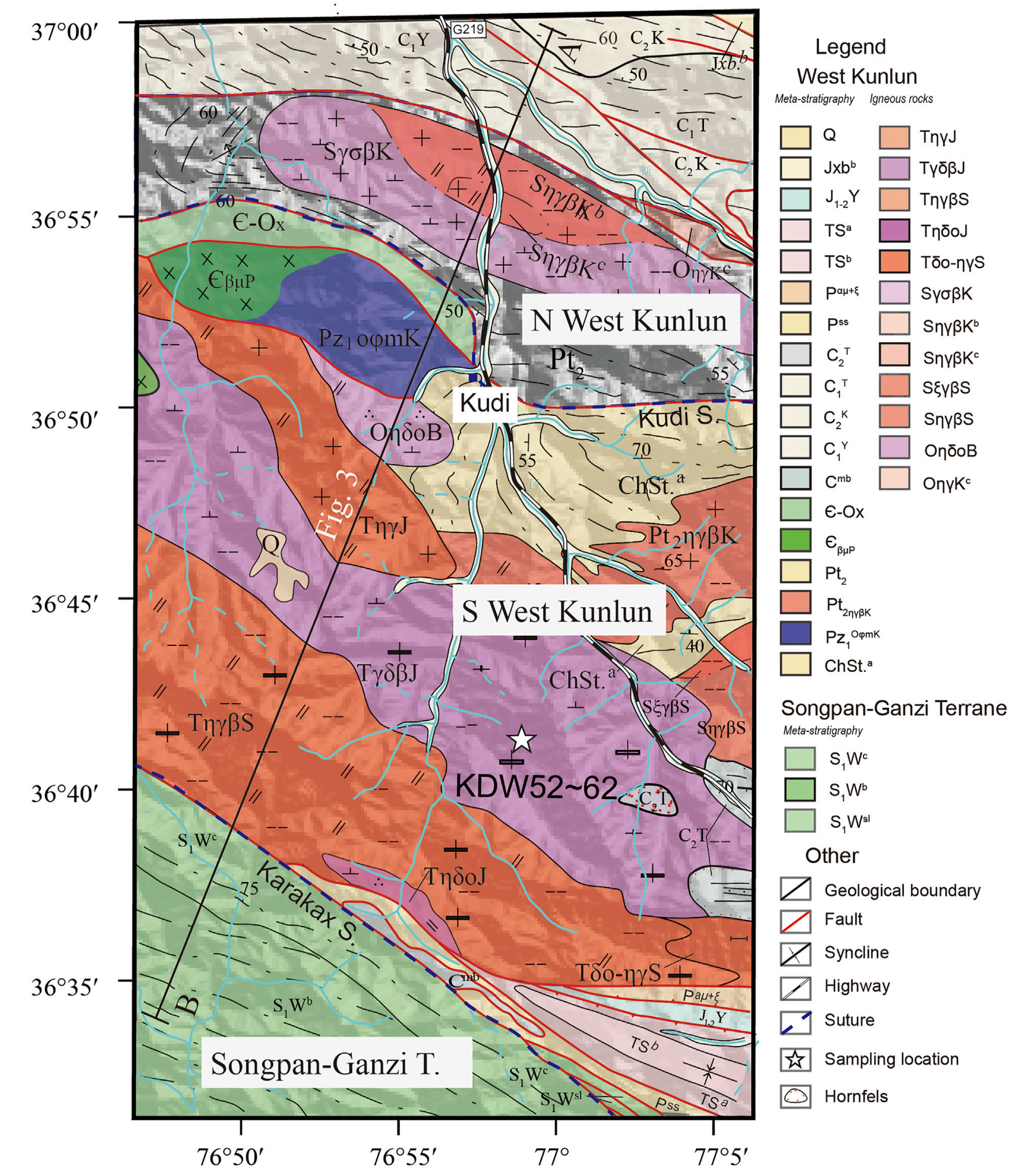

FIGURE 2 | Geological map of the corridor along the Xinjiang-Tibet Road from Akaz to Heiqia. Abbreviations for stratigraphic units are given by region. Northern West Kunlun: Pt$_2$, Middle Proterozoic; *Jxb*^{b}, segment B in the Bochatetage Formation of the Middle Proterozoic Jiexian System; C$_1^T$, Carboniferous Talong Group; C$_1^Y$, Carboniferous Yishake Group; C$_2^K$, Carboniferous Kuerliang Group; Є-Ox, Cambrian–Ordovician Xiheti Group; SγσβK, Silurian biotite adamellite; SηγβK^b, segment B in Silurian biotite adamellite; SηγβK^c, Segment C in Silurian biotite adamellite; and OηγK^c, segment C in Ordovician coarse monzogranite. Southern West Kunlun: Q, Quaternary; ChSt^a, segment A of the Saitula Group of the Middle Proterozoic Changchengian System; C$_2^t$, Carboniferous Tireaili Formation; J$_{1-2}$Y, Jurassic Yerqiang Group; P$_{z1}$OφmK, Kudi ophiolitic mélange; Pt$_{2\eta\gamma\beta K}$, Middle Proterozoic gneissic biotite monzogranite; Є$_{\beta\mu P}$, Cambrian diabase; O*ηδoB*, Ordovician medium-grained

(Continued)

FIGURE 2 | quartz diorite; Sξγβ*S*, Silurian medium-grained biotite moyite; Sηγβ*S*, Silurian medium-grained biotite monzogranite; Tηγ*J*, Triassic medium-grained monzogranite; Tγδβ*J*, Triassic medium-grained, porphyritic biotite granodiorite; Tηγβ*S*, Triassic medium-grained, porphyritic biotite monzogranite; Tηδο*J*, Triassic medium- to fine-grained quartz monzodiorite; Tδο-ηγ*S*, Triassic mixed magmatic granite; $P^{\alpha\mu+\xi}$, altered andesitic porphyrite and dacite; P^{ss}, sandstone intercalated with sericitic and silty slate; C^{mb}, bioclastic dolomitic limestone and marble; S_1W^{sl}, silty slate and phyllite; TS^a, segment A in sandstone of the Triassic Sailiyakedaban Group; and TS^b, segment A in conglomerate of the Triassic Sailiyakedaban Group. Songpan-Ganzi Terrane: S_1W^b, Formation B of the Silurian Wenquan Group, which contains gray, medium-bedded, and fine-grained arkosic sandstone intercalated with silty, *Didymites*-bearing slate; and S_1W^c, Formation C of the Silurian Wenquan Group, which contains thickly bedded, moderate- to fine-grained quartz sandstone and fine-grained arkosic sandstone intercalated with some silt and slate.

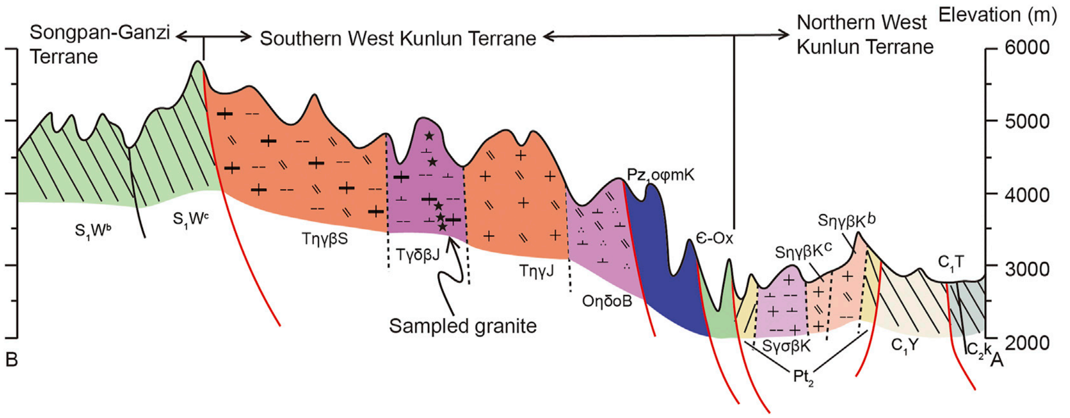

FIGURE 3 | A geological section between the Northern West Kunlun Terrane and the Songpa-Ganzi Terrane. Black stars record the elevations of samples in the Southern West Kunlun Terrane that were collected for apatite fission track analysis, although the actual locations do not lie within the plane of the section.

TABLE 1 | Apatite fission-track data of the South Kudi section in the Southern West Kunlun Terrane.

Sample	Location: Long. (E) Lat. (N)	Elevation (m)	*N*	Rho-S (10^{-5} cm^{-2}) N_s	Rho-I (10^{-5} cm^{-2}) N_i	Rho-D (10^{-5} cm^{-2}) Nd	*P*(χ^2) (%)	*Central* age (Ma) (±1σ)	Mean Dpar (μm)
KDW52	36.69767° 77.01437°	4,814	23	1.955 (98)	13.047 (654)	12.5 (16,059)	89.25	25.5 ± 3.1	1.27
KDW55	36.69469° 77.01894°	4,445	24	2.568 (212)	20.376 (1,682)	13.3 (16,059)	0.01	26.7 ± 3.2	1.36
KDW60	36.70085° 77.04183°	3,869	23	2.554 (190)	20.637 (1,535)	14.0 (16,627)	0.06	25.8 ± 3.3	1.36
KDW61	36.70045° 77.04486°	3,715	22	1.776 (148)	21.282 (1,773)	13.9 (16,627)	4.73	16.4 ± 2.0	1.26
KDW62	36.70360° 77.04749°	3,540	24	2.592 (231)	31.026 (2,765)	12.9 (16,059)	36.69	14.8 ± 1.4	1.38

The zeta (ζ) value is 272.78 ± 15.99. Abbreviations are as follows: N, *number of individual grains dated; Rho-S, spontaneous track density (×10^5 tracks cm^{-2}); Ns, number of spontaneous tracks counted; Rho-I, induced track density in external detector (muscovite) (×10^5 tracks cm^{-2}); Ni, number of induced tracks counted; Rho-D, induced track density in external detector adjacent to dosimeter glass (×10^5 tracks cm^{-2}); Nd, number of tracks used to determine Rho-D; P(χ^2) (%), Chi-square probability (Galbraith, 1984); Mean Dpar, arithmetic mean diameter of fission-track etch figures parallel to the crystallographic c-axis.*

Triassic ($T_{\gamma\delta\beta J}$) intrusion between its highest (4,814 m) and lowest (3,540 m) points (**Figures 2**, **3** and **Table 1**).

All granite samples were crushed and pulverized, and constituent minerals were concentrated by using standard magnetic and density separation techniques. Individual apatite grains were handpicked from the concentrates and used for fission track dating via the external detector method, following the procedures documented in our previous publication (Liu et al., 2017b). Initially, apatite grains were mounted and polished to expose the centers of as many grains as possible and were then immersed in 5.5 N HNO_3 for 20 s at 21°C to reveal natural fission tracks. Fission track sample mounts, age standards (Fish Canyon and Durango) and IRMM540R dosimeter samples were irradiated together in a thermalized reactor located at Oregon State University, United States, using a thermal neutron fluency of 1.0 × 10^{16} n cm^{-2}. U-free muscovite external detectors were etched in 40% HF for 40 min at 20°C to reveal their induced fission tracks. Fission tracks were counted on a Zeiss microscope at the Chinese Academy of Geological Sciences, China, using an Autoscan system (produced in

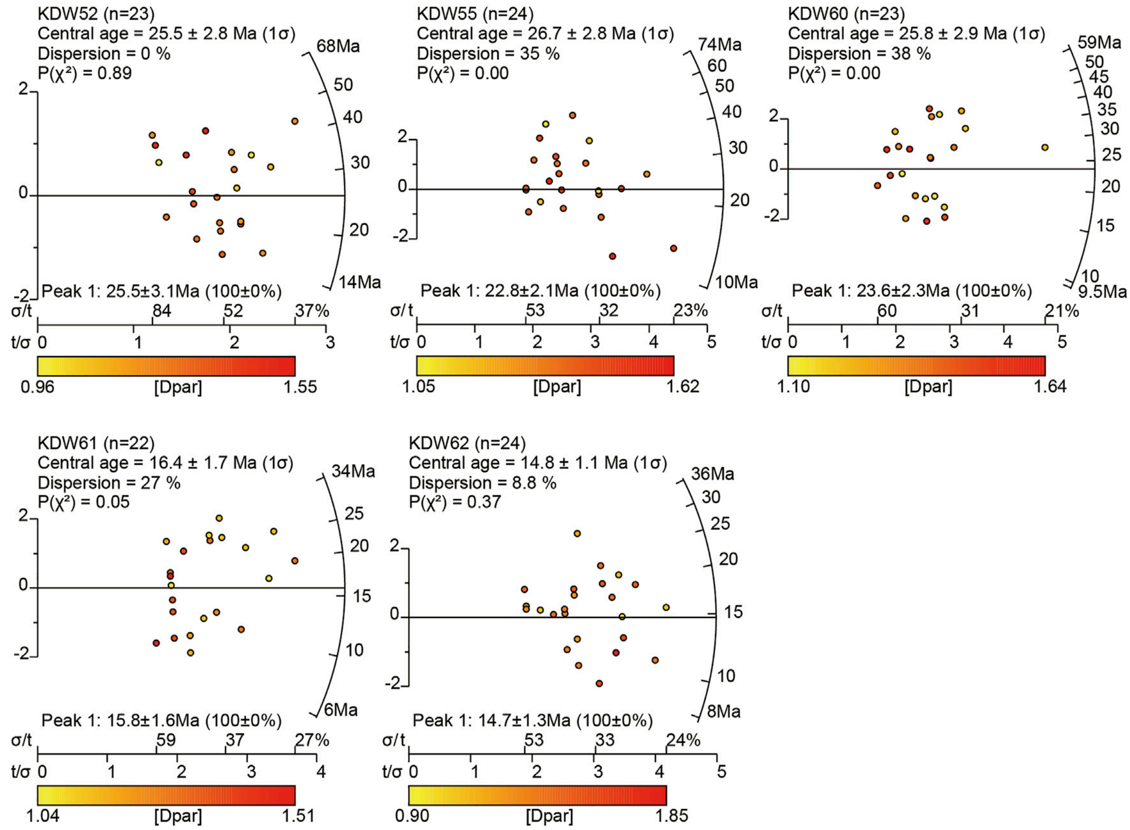

FIGURE 4 | Apatite fission track results displayed on radial plots (Galbraith, 1990) for the Kudi section. The plots were drawn using Radialplotter (Vermeesch, 2009). The color code displays uranium concentrations **(left)** or chlorine concentrations **(right)** for each sample.

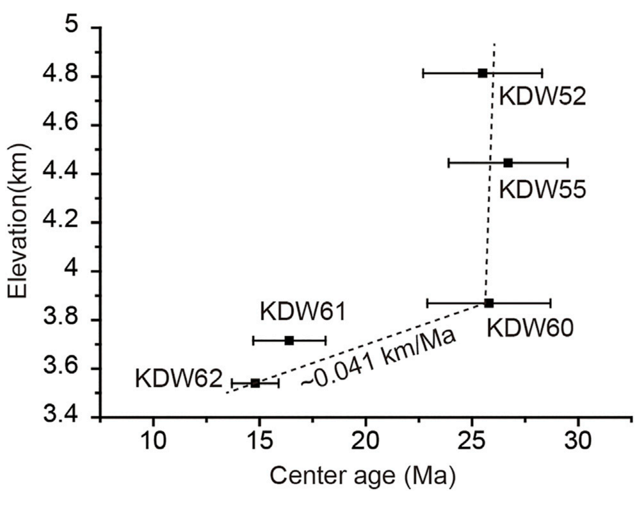

FIGURE 5 | Age–elevation relationships for apatite fission track data from the South Kudi section, with 1σ analytical uncertainties shown as error bars.

Australia) in manual mode, set to a magnification of ×1,000. The zeta (ζ) value of 272.78 ± 15.99 was obtained using Durango and Fish Canyon apatite standards (Hurford and Green, 1983; Naeser and Cebula, 1985). More than 20 grains were chosen from each sample. All ages were determined to be within an error of 1σ using the computer code "Trackkey" (Dunkl, 2002).

RESULTS

Between 22 and 24 grains were analyzed for AFT in each sample, and the results are listed in **Table 1** and shown in **Figure 4**. For this measurement, the value of Zeta (ζ) is 272.78 ± 15.99. Three samples (KDW55, KDW60 and KDW61) show low AFT P (χ^2) values (<5%), although the highest and lowest elevation samples (KDW52 and KDW62) show high P (χ^2) values (>5%) (**Table 1**). The AFT central ages are 25.5 ± 3.1, 26.7 ± 3.2, 25.8 ± 3.3, 16.4 ± 2.0, and 14.8 ± 1.4 Ma for KDW52, KDW55, KDW60, KDW61, and KDW62, respectively. The mean Dpar varied from 1.26 to 1.38 μm. Because the AFT ages determined for these samples are younger than 30 Ma, we did not measure the full track lengths.

Figure 5 shows AER data using the central ages. The ages of samples with the three highest elevations are near ~26 Ma (KDW52, KDW55 and KDW60), while the ages of the two low-elevation samples are near ~15–16 Ma (KDW61 and KDW62). A clear transition point in AER data can be seen in **Figure 5** at ~26 Ma.

DISCUSSION

Rapid Oligocene Uplift in the Southern West Kunlun Mountains

Low-temperature thermochronological data are highly effective for deciphering the cooling history of a region, with techniques including apatite (U–Th)/He (AHe, ~30–120°C), apatite fission track (AFT, ~60–110°C), zircon (U-Th)/He (ZHe, ~130–200°C), and zircon fission track (ZFT, ~220–260°C) (Reiners et al., 2005; Guenthner et al., 2013). The cooling rates, especially from the AER data, derived from these minerals have been widely used to identify rapid uplift events in the eastern (Wang et al., 2012; Tian et al., 2013; Zhang et al., 2016; Liu-Zeng et al., 2018; Cao et al., 2019; Replumaz et al., 2020), northern (Liu et al., 2017b, 2021; Wang et al., 2017; Zhuang et al., 2018; Lin et al., 2021), and western (Wang et al., 2003; Amidon and Hynek, 2010; Sobel et al., 2011; Cao et al., 2013; Thiede et al., 2013; Cao et al., 2015; Li et al., 2019) Tibetan Plateau. Unfortunately, the rapid cooling rates derived from AER data do not always imply rapid exhumation rates (Stüwe et al., 1994; Burbank, 2002). However, the break-in-slope point or zone in an AER should record a significant tectonic transformation (Braun, 2002; Valla et al., 2010), which is used to correlate with a rapid uplift event within the Tibetan Plateau (Zheng et al., 2006; Ouimet et al., 2010; Zheng et al., 2010; Lease et al., 2011; Wang et al., 2012; Tian et al., 2015). In this study, the three lowest-elevation samples yielded a mean exhumation rate of ~0.041 km/Ma. The three highest-elevation samples yield very similar central ages of ~26 Ma (**Figure 5**), indicating that the adjacent area has undergone rapid exhumation at ~26 Ma. As our samples were collected from the SWK (**Figure 1B**), the SWK is interpreted to have undergone rapid uplift at ~26 Ma, followed by a period of slow uplift that continued to at least ~15 Ma (**Figure 5**).

Based on source-to-sink theory, sedimentary provenance analysis in a basin can effectively decipher the evolutionary history of adjacent ranges (Fedo et al., 2003; Najman, 2006; Kimbrough et al., 2015; Koshnaw et al., 2018; Coutts et al., 2019; Nordsvan et al., 2020; Resentini et al., 2020). Basin analysis has been applied to several mountain fronts in the Pamir–WK region, which has constrained the evolutionary history of its adjacent ranges. The dominance of Cenozoic northward-directed paleocurrents in the SW Tarim Basin indicates that the basin sediments were mainly derived from its southern margin (Sobel, 1999; Bershaw et al., 2012; Cao et al., 2014; Zhang et al., 2019; Li et al., 2021). Interestingly, an ~45 Ma peak in detrital zircon U/Pb ages is documented only in the central Pamir and first appears in Eocene strata in the SW Tarim and Tajik basins (Blayney et al., 2016; Sun et al., 2016; Wang et al., 2019; Zhang et al., 2019; Sun et al., 2020; Wang et al., 2021). Previous documents indicated that this magmatic activity represented the Late Eocene rapid uplift in the central Pamir region, based on late Eocene detrital apatite fission track ages and regional tectonic movements (Wang et al., 2019; Zhang et al., 2019; Wang et al., 2021). Moreover, detrital zircons with an age peak of ~45 Ma are absent in sedimentary rocks that formed at ~26 Ma in the Oyitag and after ~26.5 Ma in the Aertashi sections of the SW Tarim Basin (**Figure 6**; Blayney et al., 2016; Sun et al., 2016), indicating that the influx of sediments from the central Pamir region was hindered by the growth of the mountains to the northern side of the basin. Based on our new data, we interpret that the SWK experienced rapid uplift at ~26 Ma, which restricted sediment flux into its northern basins.

Both the low-temperature thermochronology performed herein and previous basin sedimentary provenance analyses confirm that the SWK experienced rapid uplift at ~26 Ma, which restricted sediments sourced from central Pamir region from being transported into its northern basins. Paleomagnetic data show an abrupt increase in mean magnetic susceptibility at ~26 Ma in the Baxbulak section of the Alai Valley, although this has previously been interpreted as recording tectonic activity in the southwestern Tien Shan (Tang et al., 2015). Nonetheless, this rapid exhumation event (~25–16 Ma) is also documented in the northern Pamir region (Amidon and Hynek, 2010), indicating that this event may record regional-scale movement on the northwestern Tibetan Plateau.

Cenozoic Northward Growth of West Kunlun Mountains

The WK is divided into southern and northern domains, with the former extending to the northern Pamir region (**Figure 1B**). Sedimentary provenance analysis indicates that the WK and northern Pamir region had certain paleoelevations prior to the Cenozoic (Cao et al., 2015; Blayney et al., 2016; Li et al., 2020), which supports rapid uplift in the northern Pamir region during the late Paleocene–early Eocene (~50–40 Ma) (Amidon and Hynek, 2010; Carrapa et al., 2015; Chen et al., 2018). As the sedimentary provenance in the SW Tarim and Tajik basins did not change between the Late Cretaceous and the Early Eocene, the topography of the nearby ranges must also not have changed during this time. The first quasi-synchronous rapid uplift of the central Pamir region occurred in the Late Eocene (40–30 Ma), and provided a new sediment flux into the SW Tarim and Tajik basins (Blayney et al., 2016; Wang et al., 2019; Zhang et al., 2019; Sun et al., 2020; Wang et al., 2021), although this occurred at the earliest time of ~47 Ma in the Oytag section of the Tarim Basin (Sun et al., 2016). The second regional-scale rapid uplift in the SWK (this study) and northern Pamir region (Amidon and Hynek, 2010) occurred during the Oligocene; this lasted at least ~9 Ma (from 25 to 16 Ma) in the northern Pamir region, but there are no geochronological data to constrain its duration in the SWK. The >1,000-km-long Karakorum Fault developed during this Oligocene uplift event (Lacassin et al., 2004; Li et al., 2007; Valli et al., 2007; Valli et al., 2008) and subsequently played a vital role in the evolution of the WHS (Cowgill, 2010). Finally, a third episode of rapid uplift began in

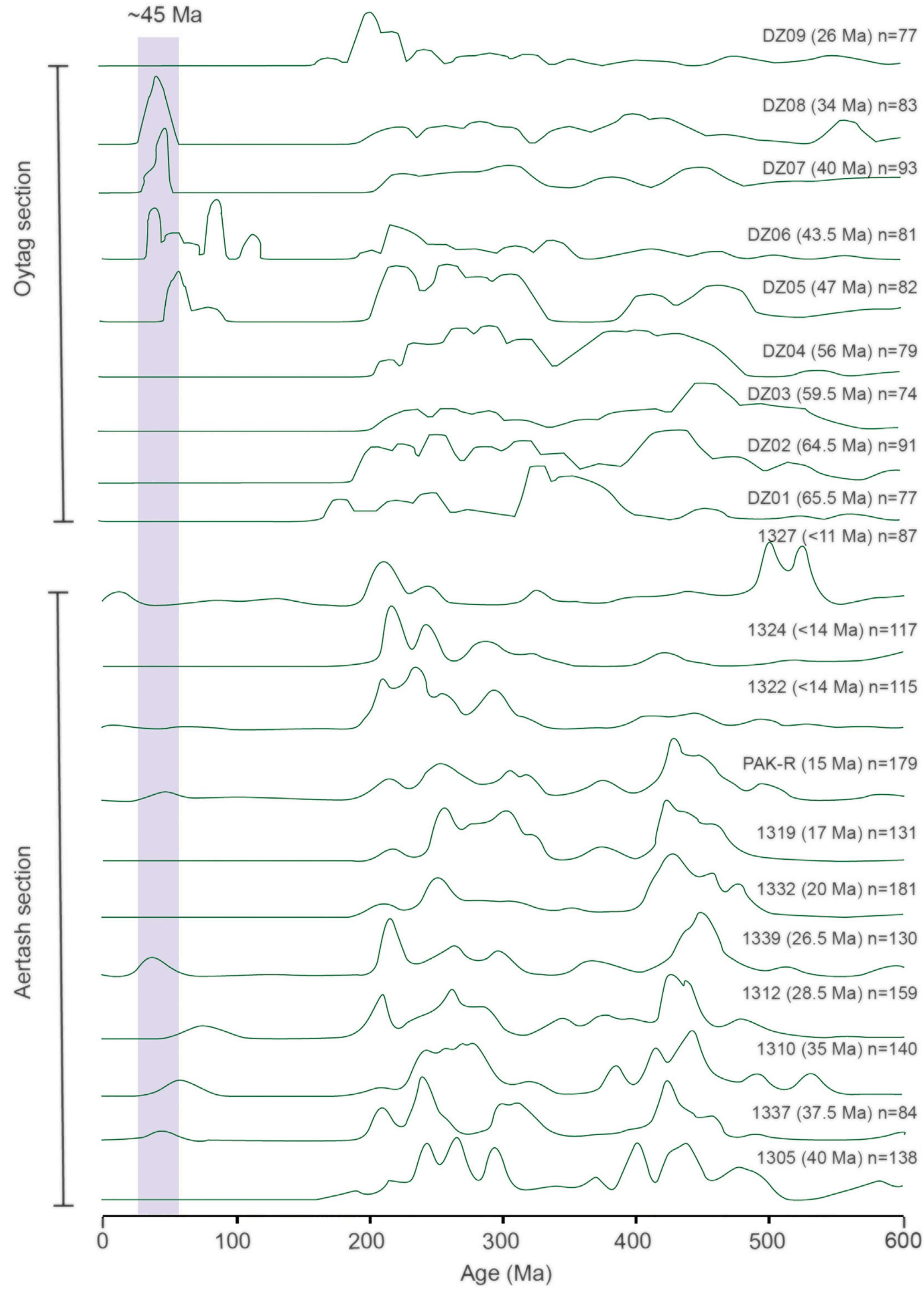

FIGURE 6 | U-Pb detrital zircon data shown as normalized kernel density plots for rocks from the Oytag (Sun et al., 2016) and Aertashi (Blayney et al., 2016) sections in the SW Tarim Basin. The shaded bar represents the populations diagnostic of the central Pamir provenance with a detrital zircon U-Pb peak age of ~45 Ma. The ages in the brackets after the sample ID represent the sedimentary ages. N indicates the number of measured detrital zircon grains.

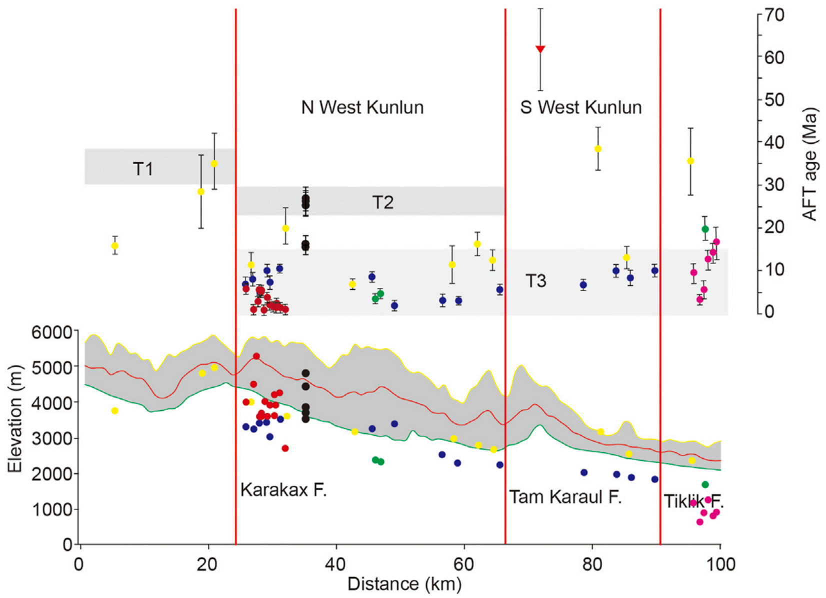

FIGURE 7 | Tectonic events that have affected the West Kunlun Mountains. Yellow, red and green lines indicate the maximum, average and minimum elevations of selected area, which showing in the **Figure 1B** with red frame. Pick dots and dots with error bars indicate the elevations and AFT cooling ages from Chapman et al. (2017). Red dots and dots with error bars indicate the elevations and AFT cooling ages from Thiede et al. (2013). Green dots and dots with error bars indicate the elevations and AFT cooling ages from Sobel et al. (2011). Blue dots and dots with error bars indicate the elevations and AFT cooling ages from Cao et al. (2013). Yellow dots and dots with error bars indicate the elevations and AFT cooling ages from Li et al. (2019). Black dots and dots with error bars indicate the elevations and AFT cooling ages from this study.

the WK and northern Pamir during the Middle Miocene, with this event continuing to the present day and shaping the current landscape (Cao et al., 2013; Thiede et al., 2013; Cao et al., 2015; Blayney et al., 2019).

Our new data combined with published results show that at least three rapid uplift events occurred in the Pamir–WK during the Cenozoic (**Figure 7**), but how did each of these events influence the tectonic evolution of the WK? The ~45 Ma peak of detrital zircon U/Pb ages indicates that the central Pamir region experienced the first uplift event, although no equivalent ages are recognized in the WK, despite its northward extension (i.e., the northern Pamir) recording this event. Moreover, if the WK had experienced this uplift at this time, the sediments from the central Pamir region would not have been deposited in the SW Tarim Basin. Therefore, we believe that the first uplift event only took place south of the WK. Our AFT data confirm that the second uplift event occurred in the SWK, which restricted sediments derived from the central Pamir region from entering the SW Tarim Basin. Prior to this study, no Oligocene thermochronological data were reported from the NWK, which implied that this second major uplift event did not affect the NWK. Furthermore, while thermochronological data confirm that the third uplift event occurred in the NWK (Sobel and Dumitru, 1997; Sobel et al., 2011; Chapman et al., 2017) and northern Pamir region (Sobel et al., 2011; Thiede et al., 2013; **Figures 1**, **7**), no previous data have shown that this event affected the SWK. Our data from the Kudi profile indicate that the phase of relatively slow exhumation lasted from ~26 to ~15 Ma (**Figure 5**). Furthermore, as the SWK currently has higher elevation than the NWK (**Figure 7**), the southern domain likely experienced a prolonged period of uplift than the northern domain. Therefore, we suggest that the SWK possibly also experienced the third documented uplift event. Based on these data, three Cenozoic uplift events should first occur to the south of the WK, SWK, and NWK during the Eocene, Oligocene, and Mid-Miocene (**Figure 7**). Therefore, northward growth should take place around the WK, possibly caused by the stepwise growth (Tapponnier et al., 2001) or continuous deformation (Molnar et al., 1993) of the Tibetan Plateau.

Sedimentary provenance analysis in the SW Tarim Basin also supports the interpreted northward growth of the WK. Detrital zircons with age peaks of ~45 Ma are absent in sedimentary rocks that formed at ~26–15 and ~14–11 Ma in the Aertashi section of the SW Tarim Basin (**Figure 6**; Blayney et al., 2016), which indicates that sediments from the central Pamir region could not freely enter its northern basin. The reason for this limited movement is most likely due to being restricted by uplift of the WK. These events are shown in **Figure 8** as a tectonic model for the WK. During the Late Cretaceous, the central Pamir–Songpan–Ganzi region had not experienced uplift, whereas the WK had a greater elevation, allowing the paleorivers (e.g., the Pishan River, the Yarkang River and others) to erode headward toward the Songpan–Ganzi terrane. During the Eocene, the Paratethys Ocean transgressed into and retreated from the Tarim Basin, and the central Pamir region experienced initial Cenozoic uplift, which allowed the paleorivers (e.g., the Pishan River and the Yarkang River) to supply new detrital zircon grains with ~45 Ma peak ages. During the Oligocene, the SWK experienced abrupt uplift, which restricted the sedimentary flux from the central Pamir region

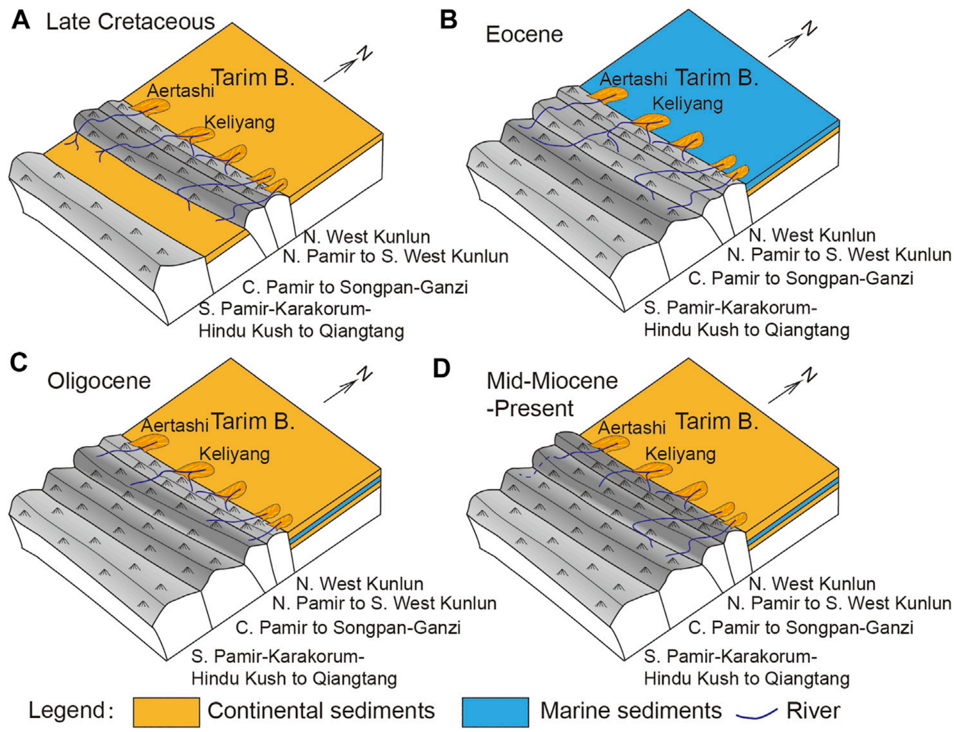

FIGURE 8 | Growth model for the region surrounding the West Kunlun Mountains. Gray value represents the paleo-altitude. During the Late Cretaceous, although the Kunlun Mountains have certain elevations, the paleorivers eroded headward toward the Songpan–Ganzi terrane **(A)**. During the Eocene, the central Pamir region experienced initial Cenozoic uplift **(B)**. During the Oligocene, the SWK experienced abrupt uplift, which was higher than the NWK and Central Pamir–Songpan–Ganzai terrane **(C)**. From the Mid-Miocene to present, the NWK and SWK both experienced abrupt uplift **(D)**.

into the SW Tarim Basin. From the middle Miocene to the present day, the NWK and SWK both experienced abrupt uplift, which restricted the transport of eroded material from the central Pamir region into the Tarim Basin, although the head of the paleo-Yarkang River eroded through the central Pamir region at ~26–15 and ~14–11 Ma.

CONCLUSION

1) The age–elevation relationship (AER) of the apatite fission track (AFT) shows that rapid exhumation occurred at ~26 Ma in southern West Kunlun.
2) Combining these data with those of previous studies shows that West Kunlun and its adjacent region experienced northward initial Cenozoic growth during the Late Eocene, Oligocene, and Middle Miocene in the central Pamir, southern West Kunlun, and northern West Kunlun regions, respectively.

DATA AVAILABILITY STATEMENT

The original contributions presented in the study are included in the article/supplementary material, further inquiries can be directed to the corresponding author.

AUTHOR CONTRIBUTIONS

This manuscript was designed and written by DL. This manuscript was supported by funds from DL, HL, and JP. The apatite fission track data were measured by YW. Other co-authors attended the field and figure work, including CG, MB, YZ, PW, FL, and SW.

FUNDING

This work was co-supported by the National Natural Science Foundation of China (41872212), the Key Special Project for Introduced Talents Team of Southern Marine Science and Engineering Guangdong Laboratory (Guangzhou) (GML2019ZD0201), the second Tibetan Plateau Scientific Expedition of the Ministry of Science and Technology of China (2019QZKK0901), the China Geological Survey project (DD20190057, DD20190059) and CSC grant (201809110053).

ACKNOWLEDGMENTS

We sincerely thank editors and two reviewers for their constructive comments. We thank GeoEditing and American Journal Experts for the entire paper review and writing improvement.

REFERENCES

Amidon, W. H., and Hynek, S. A. (2010). Exhumational History of the North Central Pamir. *Tectonics* 29, 5017. doi:10.1029/2009TC002589

Arnaud, N., Tapponnier, P., Roger, F., Brunel, M., Scharer, U., Wen, C., et al. (2003). Evidence for Mesozoic Shear Along the Western Kunlun and Altyn-Tagh Fault, Northern Tibet (China). *J. Geophys. Res.* 108, 2053. doi:10.1029/2001JB000904

Bershaw, J., Garzione, C. N., Schoenbohm, L., Gehrels, G., and Tao, L. (2012). Cenozoic Evolution of the Pamir Plateau Based on Stratigraphy, Zircon Provenance, and Stable Isotopes of Foreland basin Sediments at Oytag (Wuyitake) in the Tarim Basin (West China). *J. Asian Earth Sci.* 44, 136–148. doi:10.1016/j.jseaes.2011.04.020

Blayney, T., Dupont-Nivet, G., Najman, Y., Proust, J. N., Meijer, N., Roperch, P., et al. (2019). Tectonic Evolution of the Pamir Recorded in the Western Tarim Basin (China): Sedimentologic and Magnetostratigraphic Analyses of the Aertashi Section. *Tectonics* 38, 492–515. doi:10.1029/2018TC005146

Blayney, T., Najman, Y., Dupont-Nivet, G., Carter, A., Millar, I., Garzanti, E., et al. (2016). Indentation of the Pamirs with Respect to the Northern Margin of Tibet: Constraints from the Tarim basin Sedimentary Record. *Tectonics* 35, 2345–2369. doi:10.1002/2016tc004222

Braun, J. (2002). Quantifying the Effect of Recent Relief Changes on Age-Elevation Relationships. *Earth Planet. Sci. Lett.* 200, 331–343. doi:10.1016/S0012-821X(02)00638-6

Burbank, D. W. (2002). Rates of Erosion and Their Implications for Exhumation. *Mineral. Mag.* 66, 25–52. doi:10.1180/0026461026610014

Burtman, V. S., and Molnar, P. (1993). Geological and Geophysical Evidence for Deep Subduction of continental Crust beneath the Pamir. *Geol. Soc. Am. Spec. Pap.* 281, 1–76. doi:10.1130/spe281-p1

Cai, Z.-h., He, B., He, B.-z., Li, G.-w., Jiao, C.-l., and Yun, X.-r. (2021). Early Cretaceous Deformation in the Southern Tashkorgan Region: Implications for the Tectonic Evolution of the Northeastern Pamir. *China Geol.* 4, 61–76. doi:10.31035/cg2021023

Cao, K., Wang, G.-C., Bernet, M., van der Beek, P., and Zhang, K.-X. (2015). Exhumation History of the West Kunlun Mountains, Northwestern Tibet: Evidence for a Long-Lived, Rejuvenated Orogen. *Earth Planet. Sci. Lett.* 432, 391–403. doi:10.1016/j.epsl.2015.10.033

Cao, K., Wang, G.-C., van der Beek, P., Bernet, M., and Zhang, K.-X. (2013). Cenozoic Thermo-Tectonic Evolution of the Northeastern Pamir Revealed by Zircon and Apatite Fission-Track Thermochronology. *Tectonophysics* 589, 17–32. doi:10.1016/j.tecto.2012.12.038

Cao, K., Wang, G., Leloup, P. H., Mahéo, G., Xu, Y., van der Beek, P. A., et al. (2019). Oligocene-Early Miocene Topographic Relief Generation of Southeastern Tibet Triggered by Thrusting. *Tectonics* 38, 374–391. doi:10.1029/2017TC004832

Cao, K., Xu, Y., Wang, G., Zhang, K., van der Beek, P., Wang, C., et al. (2014). Neogene Source-To-Sink Relations between the Pamir and Tarim Basin: Insights from Stratigraphy, Detrital Zircon Geochronology, and Whole-Rock Geochemistry. *J. Geol.* 122, 433–454. doi:10.1086/676478

Carrapa, B., DeCelles, P. G., Wang, X., Clementz, M. T., Mancin, N., Stoica, M., et al. (2015). Tectono-climatic Implications of Eocene Paratethys Regression in the Tajik basin of central Asia. *Earth Planet. Sci. Lett.* 424, 168–178. doi:10.1016/j.epsl.2015.05.034

Carrapa, B., Mustapha, F. S., Cosca, M., Gehrels, G., Schoenbohm, L. M., Sobel, E. R., et al. (2014). Multisystem Dating of Modern River Detritus from Tajikistan and China: Implications for Crustal Evolution and Exhumation of the Pamir. *Lithosphere* 6, 443–455. doi:10.1130/l360.1

Chapman, J. B., Carrapa, B., Ballato, P., DeCelles, P. G., Worthington, J., Oimahmadov, I., et al. (2017). Intracontinental Subduction beneath the Pamir Mountains: Constraints from Thermokinematic Modeling of Shortening in the Tajik Fold-And-Thrust belt. *GSA Bull.* 129, 1450–1471. doi:10.1130/b31730.1

Chen, X., Chen, H., Lin, X., Cheng, X., Yang, R., Ding, W., et al. (2018). Arcuate Pamir in the Paleogene? Insights from a Review of Stratigraphy and Sedimentology of the basin Fills in the Foreland of NE Chinese Pamir, Western Tarim Basin. *Earth Sci. Rev.* 180, 1–16. doi:10.1016/j.earscirev.2018.03.003

Coutts, D. S., Matthews, W. A., and Hubbard, S. M. (2019). Assessment of Widely Used Methods to Derive Depositional Ages from Detrital Zircon Populations. *Geosci. Front.* 10, 1421–1435. doi:10.1016/j.gsf.2018.11.002

Cowgill, E. (2010). Cenozoic Right-Slip Faulting along the Eastern Margin of the Pamir Salient, Northwestern China. *Geol. Soc. Am. Bull.* 122, 145–161. doi:10.1130/B26520.1

Dunkl, I. (2002). Trackkey: a Windows Program for Calculation and Graphical Presentation of Fission Track Data. *Comput. Geosci.* 28, 3–12. doi:10.1016/S0098-3004(01)00024-3

Fedo, C. M., Sircombe, K. N., and Rainbird, R. H. (2003). Detrital Zircon Analysis of the Sedimentary Record. *Rev. Mineral. Geochem.* 53, 277–303. doi:10.2113/0530277

Galbraith, R. F. (1984). On Statistical Estimation in Fission Track Dating. *J. Int. Assoc. Math. Geol.* 16, 653–669. doi:10.1007/BF01033028

Galbraith, R. (1990). The Radial Plot: Graphical Assessment of Spread in Ages. *Nucl. Tracks Radiat. Meas.* 17, 207–214. doi:10.1016/1359-0189(90)90036-W

Guenthner, W. R., Reiners, P. W., Ketcham, R. A., Nasdala, L., and Giester, G. (2013). Helium Diffusion in Natural Zircon: Radiation Damage, Anisotropy, and the Interpretation of Zircon (U-Th)/He Thermochronology. *Am. J. Sci.* 313, 145–198. doi:10.2475/03.2013.01

Hu, X., Garzanti, E., Wang, J., Huang, W., An, W., and Webb, A. (2016). The Timing of India-Asia Collision Onset - Facts, Theories, Controversies. *Earth-Science Rev.* 160, 264–299. doi:10.1016/j.earscirev.2016.07.014

Hurford, A. J., and Green, P. F. (1983). The Zeta Age Calibration of Fission-Track Dating. *Chem. Geol.* 41, 285–317. doi:10.1016/S0009-2541(83)80026-6

Jia, C., Zhang, S. B., and Wu, S. Z. (2004). *Stratigraphy of the Tarim Basin and Adjacent Area*. Beijing: Science Press.

Jiang, X.-D., and Li, Z.-X. (2014). Seismic Reflection Data Support Episodic and Simultaneous Growth of the Tibetan Plateau since 25 Myr. *Nat. Commun.* 5, 5453. doi:10.1038/ncomms6453

Jiang, X., Li, Z.-X., and Li, H. (2013). Uplift of the West Kunlun Range, Northern Tibetan Plateau, Dominated by Brittle Thickening of the Upper Crust. *Geology* 41, 439–442. doi:10.1130/G33890.1

Kimbrough, D. L., Grove, M., Gehrels, G. E., Dorsey, R. J., Howard, K. A., Lovera, O., et al. (2015). Detrital Zircon U-Pb Provenance of the Colorado River: A 5 m.Y. Record of Incision into Cover Strata Overlying the Colorado Plateau and Adjacent Regions. *Geosphere* 11, 1719–1748. doi:10.1130/GES00982.1

Koshnaw, R. I., Stockli, D. F., and Schlunegger, F. (2018). Timing of the Arabia-Eurasia continental Collision-Evidence from Detrital Zircon U-Pb Geochronology of the Red Bed Series Strata of the Northwest Zagros Hinterland, Kurdistan Region of Iraq. *Geology* 47, 47–50. doi:10.1130/g45499.1

Laborde, A., Barrier, L., Simoes, M., Li, H., Coudroy, T., Van der Woerd, J., et al. (2019). Cenozoic Deformation of the Tarim Basin and Surrounding Ranges (Xinjiang, China): A Regional Overview. *Earth Sci. Rev.* 197, 102891. doi:10.1016/j.earscirev.2019.102891

Lacassin, R., Valli, F., Arnaud, N., Leloup, P. H., Paquette, J. L., Haibing, L., et al. (2004). Large-scale Geometry, Offset and Kinematic Evolution of the Karakorum Fault, Tibet. *Earth Planet. Sci. Lett.* 219, 255–269. doi:10.1016/S0012-821X(04)00006-8

Lease, R. O., Burbank, D. W., Clark, M. K., Farley, K. A., Zheng, D., and Zhang, H. (2011). Middle Miocene Reorganization of Deformation along the Northeastern Tibetan Plateau. *Geology* 39, 359–362. doi:10.1130/g31356.1

Leech, M., Singh, S., Jain, A., Klemperer, S., and Manickavasagam, R. (2005). The Onset of India-Asia continental Collision: Early, Steep Subduction Required by the Timing of UHP Metamorphism in the Western Himalaya. *Earth Planet. Sci. Lett.* 234, 83–97. doi:10.1016/j.epsl.2005.02.038

Li, C., Chen, H., Zhang, F., Lin, X., Cheng, X., Li, Y., et al. (2021). Cenozoic basin-filling Evolution of the SW Tarim Basin and its Implications for the Uplift of Western Kunlun: Insights from (Seismo)stratigraphy. *Palaeogeogr. Palaeoclimatol. Palaeoecol.* 562, 110149. doi:10.1016/j.palaeo.2020.110149

Li, G., Sandiford, M., Fang, A., Kohn, B., Sandiford, D., Fu, B., et al. (2019). Multi-stage Exhumation History of the West Kunlun Orogen and the Amalgamation of the Tibetan Plateau. *Earth Planet. Sci. Lett.* 528, 115833. doi:10.1016/j.epsl.2019.115833

Li, H., Valli, F., Liu, D., Xu, Z., Yang, J., Arnaud, N., et al. (2007). Initial Movement of the Karakorum Fault in Western Tibet: Constraints from SHRIMP U-Pb Dating of Zircons. *Chin. Sci. Bull.* 52, 1089–1100. doi:10.1007/s11434-007-0164-6

Li, Y.-P., Robinson, A. C., Gadoev, M., and Oimuhammadzoda, I. (2020). Was the Pamir Salient Built along a Late Paleozoic Embayment on the Southern Asian Margin? *Earth Planet. Sci. Lett.* 550, 116554. doi:10.1016/j.epsl.2020.116554

Lin, X., Jolivet, M., Liu-Zeng, J., Cheng, F., Tian, Y., and Li, C. a. (2021). Mesozoic-Cenozoic Cooling History of the Eastern Qinghai Nan Shan (NW China): Apatite Low-Temperature Thermochronology Constraints. *Palaeogeogr. Palaeoclimatol. Palaeoecol.* 572, 110416. doi:10.1016/j.palaeo.2021.110416

Liu, D., Li, H., Chevalier, M.-L., Sun, Z., Pei, J., Pan, J., et al. (2021). Activity of the Baiganhu Fault of the Altyn Tagh Fault System, Northern Tibetan Plateau: Insights from Zircon and Apatite Fission Track Analyses. *Palaeogeogr. Palaeoclimatol. Palaeoecol.* 570, 110356. doi:10.1016/j.palaeo.2021.110356

Liu, D., Li, H., Sun, Z., Cao, Y., Wang, L., Pan, J., et al. (2017a). Cenozoic Episodic Uplift and Kinematic Evolution between the Pamir and Southwestern Tien Shan. *Tectonophysics* 712–713, 438–454. doi:10.1016/j.tecto.2017.06.009

Liu, D., Li, H., Sun, Z., Pan, J., Wang, M., Wang, H., et al. (2017b). AFT Dating Constrains the Cenozoic Uplift of the Qimen Tagh Mountains, Northeast Tibetan Plateau, Comparison with LA-ICPMS Zircon U-Pb Ages. *Gondwana Res.* 41, 438–450. doi:10.1016/j.gr.2015.10.008

Liu-Zeng, J., Zhang, J., McPhillips, D., Reiners, P., Wang, W., Pik, R., et al. (2018). Multiple Episodes of Fast Exhumation since Cretaceous in Southeast Tibet, Revealed by Low-Temperature Thermochronology. *Earth Planet. Sci. Lett.* 490, 62–76. doi:10.1016/j.epsl.2018.03.011

Matte, P., Tapponnier, P., Arnaud, N., Bourjot, L., Avouac, J., Vidal, P., et al. (1996). Tectonics of Western Tibet, between the Tarim and the Indus. *Earth Planet. Sci. Lett.* 142, 311–330. doi:10.1016/0012-821X(96)00086-6

Molnar, P., England, P., and Martinod, J. (1993). Mantle Dynamics, Uplift of the Tibetan Plateau, and the Indian Monsoon. *Rev. Geophys.* 31, 357–396. doi:10.1029/93RG02030

Naeser, C. W., and Cebula, G. T. (1985). Re-collection of Fish Canyon Tuff for Fission-Track Standardization. *Nucl. Tracks Radiat. Meas.* 10, 393. doi:10.1016/0735-245X(85)90128-0

Najman, Y. (2005). The Detrital Record of Orogenesis: A Review of Approaches and Techniques Used in the Himalayan Sedimentary Basins. *Earth-Science Rev.* 74, 1–72. doi:10.1016/j.earscirev.2005.04.004

Nordsvan, A. R., Kirscher, U., Kirkland, C. L., Barham, M., and Brennan, D. T. (2020). Resampling (Detrital) Zircon Age Distributions for Accurate Multidimensional Scaling Solutions. *Earth Sci. Rev.* 204, 103149. doi:10.1016/j.earscirev.2020.103149

Ouimet, W., Whipple, K., Royden, L., Reiners, P., Hodges, K., and Pringle, M. (2010). Regional Incision of the Eastern Margin of the Tibetan Plateau. *Lithosphere* 2, 50–63. doi:10.1130/L57.1

Raymo, M. E., and Ruddiman, W. F. (1992). Tectonic Forcing of Late Cenozoic Climate. *Nature* 359, 117–122. doi:10.1038/359117a0

Reiners, P. W., Ehlers, T. A., and Zeitler, P. K. (2005). Past, Present, and Future of Thermochronology. *Rev. Mineral. Geochem.* 58, 1–18. doi:10.2138/rmg.2005.58.1

Replumaz, A., San José, M., Margirier, A., Beek, P., Gautheron, C., Leloup, P. H., et al. (2020). Tectonic Control on Rapid Late Miocene-Quaternary Incision of the Mekong River Knickzone, Southeast Tibetan Plateau. *Tectonics* 39, e2019TC005782. doi:10.1029/2019TC005782

Resentini, A., Andò, S., Garzanti, E., Malusà, M. G., Pastore, G., Vermeesch, P., et al. (2020). Zircon as a Provenance Tracer: Coupling Raman Spectroscopy and U Pb Geochronology in Source-To-Sink Studies. *Chem. Geol.* 555, 119828. doi:10.1016/j.chemgeo.2020.119828

Robinson, A. C., Yin, A., Manning, C. E., Harrison, T. M., Zhang, S.-H., and Wang, X.-F. (2007). Cenozoic Evolution of the Eastern Pamir: Implications for Strain-Accommodation Mechanisms at the Western End of the Himalayan-Tibetan Orogen. *Geol. Soc. Am. Bull.* 119, 882–896. doi:10.1130/b25981.1

Robinson, A. C., Yin, A., Manning, C. E., Harrison, T. M., Zhang, S.-H., and Wang, X.-F. (2004). Tectonic Evolution of the Northeastern Pamir: Constraints from the Northern Portion of the Cenozoic Kongur Shan Extensional System, Western China. *Geol. Soc. Am. Bull.* 116, 953–973. doi:10.1130/b25375.1

Royden, L. H., Burchfiel, B. C., and van der Hilst, R. D. (2008). The Geological Evolution of the Tibetan Plateau. *Science* 321, 1054–1058. doi:10.1126/science.1155371

Sakuma, A., Tada, R., Yoshida, T., Hasegawa, H., Sugiura, N., Karasuda, A., et al. (2021). Relationship between Tectonism and Desertification Inferred from Provenance and Lithofacies Changes in the Cenozoic Terrestrial Sequence of the Southwestern Tarim Basin. *Prog. Earth Planet. Sci.* 8, 44. doi:10.1186/s40645-021-00427-6

Sobel, E. R. (1999). Basin Analysis of the Jurassic-Lower Cretaceous Southwest Tarim basin, Northwest China. *GSA Bull.* 111, 709–724. doi:10.1130/0016-7606(1999)111<0709:baotjl>2.3.co;2

Sobel, E. R., and Dumitru, T. A. (1997). Thrusting and Exhumation Around the Margins of the Western Tarim basin during the India-Asia Collision. *J. Geophys. Res.* 102, 5043–5063. doi:10.1029/96JB03267

Sobel, E. R., Schoenbohm, L. M., Chen, J., Thiede, R., Stockli, D. F., Sudo, M., et al. (2011). Late Miocene-Pliocene Deceleration of Dextral Slip between Pamir and Tarim: Implications for Pamir Orogenesis. *Earth Planet. Sci. Lett.* 304, 369–378. doi:10.1016/j.epsl.2011.02.012

Stüwe, K., White, L., and Brown, R. (1994). The Influence of Eroding Topography on Steady-State Isotherms. Application to Fission Track Analysis. *Earth Planet. Sci. Lett.* 124, 63–74. doi:10.1016/0012-821X(94)00068-9

Sun, J., Xiao, W., Windley, B. F., Ji, W., Fu, B., Wang, J., et al. (2016). Provenance Change of Sediment Input in the Northeastern Foreland of Pamir Related to Collision of the Indian Plate with the Kohistan-Ladakh Arc at Around 47 Ma. *Tectonics* 35, 315–338. doi:10.1002/2015TC003974

Sun, J., Zhang, Z., Cao, M., Windley, B. F., Tian, S., Sha, J., et al. (2020). Timing of Seawater Retreat from Proto-Paratethys, Sedimentary Provenance, and Tectonic Rotations in the Late Eocene-Early Oligocene in the Tajik Basin, Central Asia. *Palaeogeogr. Palaeoclimatol. Palaeoecol.* 545, 109657. doi:10.1016/j.palaeo.2020.109657

Tang, Z., Dong, X., Wang, X., and Ding, Z. (2015). Oligocene-Miocene Magnetostratigraphy and Magnetic Anisotropy of theBaxbulak Section from thePamir-TianShan Convergence Zone. *Geochem. Geophys. Geosyst.* 16, 3575–3592. doi:10.1002/2015GC005965

Tapponnier, P., Zhiqin, X., Roger, F., Meyer, B., Arnaud, N., Wittlinger, G., et al. (2001). Oblique Stepwise Rise and Growth of the Tibet Plateau. *Science* 294, 1671–1677. doi:10.1126/science.105978

Thiede, R. C., Sobel, E. R., Chen, J., Schoenbohm, L. M., Stockli, D. F., Sudo, M., et al. (2013). Late Cenozoic Extension and Crustal Doming in the India-Eurasia Collision Zone: New Thermochronologic Constraints from the NE Chinese Pamir. *Tectonics* 32, 763–779. doi:10.1002/tect.20050

Tian, Y., Kohn, B. P., Gleadow, A. J. W., and Hu, S. (2013). Constructing the Longmen Shan Eastern Tibetan Plateau Margin: Insights from Low-Temperature Thermochronology. *Tectonics* 32, 576–592. doi:10.1002/tect.20043

Tian, Y., Kohn, B. P., Hu, S., and Gleadow, A. J. W. (2015). Synchronous Fluvial Response to Surface Uplift in the Eastern Tibetan Plateau: Implications for Crustal Dynamics. *Geophys. Res. Lett.* 42, 29–35. doi:10.1002/2014GL062383

Valla, P. G., Herman, F., van der Beek, P. A., and Braun, J. (2010). Inversion of Thermochronological Age-Elevation Profiles to Extract Independent Estimates of Denudation and Relief History - I: Theory and Conceptual Model. *Earth Planet. Sci. Lett.* 295, 511–522. doi:10.1016/j.epsl.2010.04.033

Valli, F., Arnaud, N., Leloup, P. H., Sobel, E. R., Mahéo, G., Lacassin, R., et al. (2007). Twenty Million Years of Continuous Deformation along the Karakorum Fault, Western Tibet: A Thermochronological Analysis. *Tectonics* 26, TC4004. doi:10.1029/2005TC001913

Valli, F., Leloup, P. H., Paquette, J.-L., Arnaud, N., Li, H., Tapponnier, P., et al. (2008). New U-Th/Pb Constraints on Timing of Shearing and Long-Term Slip-Rate on the Karakorum Fault. *Tectonics* 27, TC5007. doi:10.1029/2007TC002184

Vermeesch, P. (2009). RadialPlotter: A Java Application for Fission Track, Luminescence and Other Radial Plots. *Radiat. Meas.* 44, 409–410. doi:10.1016/j.radmeas.2009.05.003

Wang, E., Kirby, E., Furlong, K. P., van Soest, M., Xu, G., Shi, X., et al. (2012). Two-phase Growth of High Topography in Eastern Tibet during the Cenozoic. *Nat. Geosci.* 5, 640–645. doi:10.1038/ngeo1538

Wang, E., Wan, J. L., and Liu, J. Q. (2003). Late Cenozoic Geological Evolution of the Foreland basin Bordering the West Kunlun Range in Pulu Area: Constraints on Timing of Uplift of Northern Margin of the Tibetan Plateau. *J. Geophys. Res.* 108, 2401. doi:10.1029/2002JB001877

Wang, F., Shi, W., Zhang, W., Wu, L., Yang, L., Wang, Y., et al. (2017). Differential Growth of the Northern Tibetan Margin: Evidence for Oblique Stepwise Rise of the Tibetan Plateau. *Sci. Rep.* 7, 41164. doi:10.1038/srep41164

Wang, G., Cao, K., Zhang, K., Wang, A., Liu, C., Meng, Y., et al. (2011). Spatio-Temporal Framework of Tectonic Uplift Stages of the Tibetan Plateau in Cenozoic. *Sci. China Earth Sci.* 54, 29–44. doi:10.1007/s11430-010-4110-0

Wang, P., Liu, D., Li, H., Chevalier, M.-L., Wang, Y., Pan, J., et al. (2021). Sedimentary Provenance Changes Constrain the Eocene Initial Uplift of the Central Pamir, NW Tibetan Plateau. *Front. Earth Sci.* 9, 741194. doi:10.3389/feart.2021.741194

Wang, X., Carrapa, B., Chapman, J. B., Henriquez, S., Wang, M., DeCelles, P. G., et al. (2019). Parathethys Last Gasp in Central Asia and Late Oligocene Accelerated Uplift of the Pamirs. *Geophys. Res. Lett.* 46, 11773–11781. doi:10.1029/2019GL084838

Yin, A., and Harrison, T. M. (2000). Geologic Evolution of the Himalayan-Tibetan Orogen. *Annu. Rev. Earth Planet. Sci.* 28, 211–280. doi:10.1146/annurev.earth.28.1.211

Zhang, H., Oskin, M. E., Liu-Zeng, J., Zhang, P., Reiners, P. W., and Xiao, P. (2016). Pulsed Exhumation of Interior Eastern Tibet: Implications for Relief Generation Mechanisms and the Origin of High-Elevation Planation Surfaces. *Earth Planet. Sci. Lett.* 449, 176–185. doi:10.1016/j.epsl.2016.05.048

Zhang, S., Hu, X., and Garzanti, E. (2019). Paleocene Initial Indentation and Early Growth of the Pamir as Recorded in the Western Tarim Basin. *Tectonophysics* 772, 228207. doi:10.1016/j.tecto.2019.228207

Zheng, D., Clark, M. K., Zhang, P., Zheng, W., and Farley, K. A. (2010). Erosion, Fault Initiation and Topographic Growth of the North Qilian Shan (Northern Tibetan Plateau). *Geosphere* 6, 937–941. doi:10.1130/GES00523.1

Zheng, D., Zhang, P.-Z., Wan, J., Yuan, D., Li, C., Yin, G., et al. (2006). Rapid Exhumation at ~8 Ma on the Liupan Shan Thrust Fault from Apatite Fission-Track Thermochronology: Implications for Growth of the Northeastern Tibetan Plateau Margin. *Earth Planet. Sci. Lett.* 248, 198–208. doi:10.1016/j.epsl.2006.05.023

Zhuang, G., Johnstone, S. A., Hourigan, J., Ritts, B., Robinson, A., and Sobel, E. R. (2018). Understanding the Geologic Evolution of Northern Tibetan Plateau with Multiple Thermochronometers. *Gondwana Res.* 58, 195–210. doi:10.1016/j.gr.2018.02.014

Conflict of Interest: The authors declare that the research was conducted in the absence of any commercial or financial relationships that could be construed as a potential conflict of interest.

Publisher's Note: All claims expressed in this article are solely those of the authors and do not necessarily represent those of their affiliated organizations, or those of the publisher, the editors and the reviewers. Any product that may be evaluated in this article, or claim that may be made by its manufacturer, is not guaranteed or endorsed by the publisher.